Received 16 October 2018; accepted 19 October 2018. Date of publication 23 October 2018; date of current version 1 March 2019.
The review of this paper was arranged by Editor M. Östling.

Digital Object Identifier 10.1109/JEDS.2018.2877495

Dynamic Switching Characteristics of 1 A Forward Current β-Ga_2O_3 Rectifiers

JIANCHENG YANG [1], FAN REN [1] (Fellow, IEEE), YEN-TING CHEN [2], YU-TE LIAO [2] (Member IEEE), CHIN-WEI CHANG [3], JENSHAN LIN [3] (Fellow, IEEE), MARKO J. TADJER [4] (Senior Member, IEEE), S. J. PEARTON [5] (Fellow, IEEE), AND AKITO KURAMATA [6]

1 Department of Chemical Engineering, University of Florida, Gainesville, FL 32611, USA
2 Department of Electrical and Computer Engineering, National Chiao Tung University, Hsinchu 30010, Taiwan
3 Department of Electrical and Computer Engineering, University of Florida, Gainesville, FL 32611, USA
4 Power Electronics Section, Naval Research Laboratory, Washington, DC 20375, USA
5 Department of Materials Science and Engineering, University of Florida, Gainesville, FL 32611, USA
6 Crystal Growth Division, Tamura Corporation and Novel Crystal Technology, Inc., Saitama 350-1328, Japan

CORRESPONDING AUTHOR: S. J. PEARTON (e-mail: spear@mse.ufl.edu)

The work of J. Yang, F. Ren, C.-W. Chang, J. Lin, and S. J. Pearton was supported by the Department of the Defense, Defense Threat Reduction Agency under Grant HDTRA1-17-1- 011, monitored by Jacob Calkins. The work of M. J. Tadjer was supported by the Office of Naval Research, under Contract N00014-15-1-2392. The work of A. Kuramata was supported by ONR Global under Grant N62909-16-1-2217.

ABSTRACT An inductive load test circuit was used to measure the switching performance of field-plated edge-terminated Schottky rectifiers with a reverse breakdown voltage of 760 V (0.1 cm diameter, $7.85 \times 10^{-3}cm^2$ area) and an absolute forward current of 1 A on 8 μm thick epitaxial β-Ga_2O_3 drift layers. The recovery characteristics for these vertical geometry β-Ga_2O_3 Schottky rectifiers switching from forward current of 1 A to reverse off-state voltage of −300 V showed a recovery time (trr) of 64 ns. There was no significant temperature dependence of trr up to 150 °C.

INDEX TERMS Gallium oxide, Schottky diode, rectifiers.

I. INTRODUCTION

There is strong interest in the application of wide-bandgap semiconductors to power device applications to overcome the limitations of Si with respect to blocking voltage, maximum operating temperature and switching frequency. Improved power efficiency and densities are achieved with commercially available SiC (bandgap 3.3 eV) and GaN (bandgap 3.4 eV) rectifiers in switching and control applications [1]–[3]. Recently, β-Ga_2O_3, with its even higher theoretical power figure-of-merit, has attracted attention for achieving even higher blocking voltages and lower on-resistance due to its higher band gap of 4.8 eV, which corresponds to a ~8 MV/cm theoretical breakdown electric field [4]–[20]. Reverse breakdown voltages larger than 1 kV were reported for both unterminated Ga_2O_3 vertical rectifiers (1000-1600 V) and field-plated Schottky diodes (1076-2300 V) with an epi thickness of 8-20 μm [10]–[12], [14], [19] Furthermore, the switching characteristics of discrete Ga_2O_3 vertical Schottky rectifiers were also investigated, and the recovery time was in the range of 20 to 30 ns [10], [12], [13]. Joishi *et al.* [20] reported field-plate bevel mesa Schottky diodes using LPCVD-grown β-Ga_2O_3 epi layers. The devices had maximum reverse breakdown of 190V, corresponding to a breakdown field of $4.2MV.cm^{-1}$, with an extrinsic R_{ON} of 3.9 $m\Omega\cdot cm^2$. the absence of clear demonstrations of p-type doping in Ga_2O_3, which may be a fundamental issue resulting from the band structure, makes it difficult to simultaneously achieve low turn-on voltages and ultra-high breakdown because of the absence of a p-i-n rectifier technology.

Mixed-mode circuit simulations of Ga_2O_3 power MOSFETs have shown lower conduction loss and higher switching loss than commercial SiC MOSFETs in a three phase modular multilevel converter [21], [22]. Experimental measurements of Ga_2O_3 device switching performance are needed to optimize design and reducing switching loss.

2168-6734 © 2018 IEEE. Translations and content mining are permitted for academic research only.
Personal use is also permitted, but republication/redistribution requires IEEE permission.
See http://www.ieee.org/publications_standards/publications/rights/index.html for more information.

He *et al.* [23] evaluated dynamic behavior of 200V breakdown Ga_2O_3 diodes for switching operations induced by half-wave rectification (100 kHz) in an AC-DC converter circuit and found performance comparable to SiC [24]. It is clear that the performance of Ga_2O_3 rectifiers is improving rapidly [17], but more work is needed for high current switching conditions. Takatsuka *et al.* [25] reported the recovery characteristics of β-Ga_2O_3 trench MOS Schottky barrier diodes with chip size 0.9 × 0.9 mm^2, active region diameter 0.3 mm, specific on-resistance *Ron* of 3.09 mΩ·cm^2 and breakdown voltage 300 V. They obtained reverse recovery times of order 7 ns for switching from 1A forward current to −100 V reverse voltage, faster than Si or SiC diodes [25].

In this letter, we report the temperature dependence of reverse recovery times of larger area, 1A Ga_2O_3 field-plated rectifiers fabricated on 8 μm epitaxial layers on bulk conducting substrates using an inductive load test circuit. We demonstrate that these devices switched from 1A forward current to −300V reverse bias exhibit high switching speed and low loss recovery characteristics.

II. EXPERIMENTAL

Drift layers of Si doped n-type Ga_2O_3 with epitaxial layer thickness 8 μm were grown by Halide Vapor Epitaxy (HVPE) on β-phase Sn-doped Ga_2O_3 single crystal wafers with (001) surface orientation. These bulk wafers were grown by the edge-defined film-fed method with a carrier concentration of 3.6 × 10^{18} cm^{-3}. The field-plated, edge terminated (FPET) vertical rectifier fabrication started with full back-side Ti/Au Ohmic contacts, followed by rapid thermal annealing under N_2 at 550°C for 30 sec [14], [15]. A combination of SiO_2/SiN_x dielectric layers (40/360 nm) were deposited using plasma enhanced chemical vapor deposition. Different size dielectric windows were etched with 1:10 buffered oxide etch (BOE). Ni/Au Schottky contacts (thickness 80 nm/420 nm) were deposited on the dielectric windows with 10μm overlap with the SiO_2/SiN_x dielectric layer. The diameter of the circular contact was 0.1 cm (area 7.85 × 10^{-3} cm^2). Figure 1 shows the cross-sectional schematic of the rectifier. Diode DC characteristics were carried out with an Agilent 4156C parameter analyzer for current and voltage level up to 100 mA and 100 V, respectively. For high voltage and current DC measurements, a Tektronix 370A curve tracer was used. A current probe along with a Micsig (DP10013) differential probe was used for the diode switching characteristic measurements.

To measure the response of the diode's recovery time, a clamped inductive load test circuit was designed and fabricated for the switching measurement [21], [22], Figure 2. The circuit operations are also illustrated. During the switching operation, a double pulse was employed to drive the Si transistor, and the duration of the duty cycle was used to adjust the Ga_2O_3 Schottky diode forward current. First, the inductor was charged from the DC power supply when the transistor was turned on (accumulation mode). When the transistor was turned off, the pre-charged inductor released charge through the forward-biased diode (circulating mode). As the transistor turned on again, the Schottky diode was switched from the on- to the off- state, where the charge in the diode was depleted. Finally, the current through the diode becomes zero. The schematic of the reverse recovery output represents that direction of the current flow under different pulse period for the circuit board. Both inductor and Si MOSFET were purchased from Mouser Electronics. The inductor that was used for this circuit has inductance of 15 mH with maximum DC current of 1.3 A. The model number for Si MOSFET is STW9N150 with 1500 V of drain-source breakdown, 8 A of continuous drain current, and 2.5 Ω drain-source resistance. There was no simulation on the actual device reverse recovery characteristics for this study. A photo of the entire test set-up is shown in Figure 3.

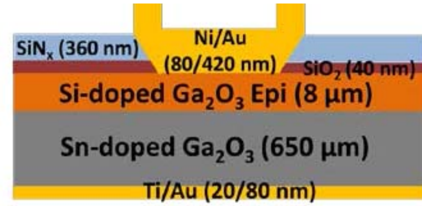

FIGURE 1. Schematic of field-plated rectifier.

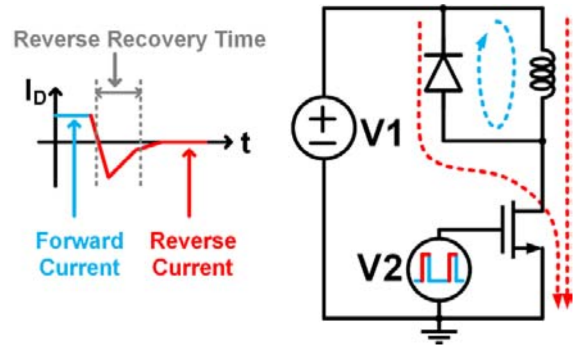

FIGURE 2. (left) The simulated reverse recovery output for a certain time scale and (right) clamped inductive load test circuit for testing switching characteristics operation of circuit during forward and reverse current operation of rectifier.

III. RESULTS AND DISCUSSION

Figure 4 shows the single-sweep forward and reverse current density (J-V) characteristics for the rectifier. The breakdown voltage (V_B) was 760 V, with 1A of forward current at ∼2.3V. The current density for this 1 A device is in the range of 127 A/cm^2, which is lower than the smaller devices on this sample. We believe that this is mainly due to the spreading resistance of our Schottky contact for a larger device size. The leakage current at lower reverse voltage is a result of the measurement limitation of the curve tracer of around 10 nA resolution. The thermionic emission model was used to obtain Schottky barrier height and ideality factor of 1.05 eV and 1.08, respectively. The carrier concentration

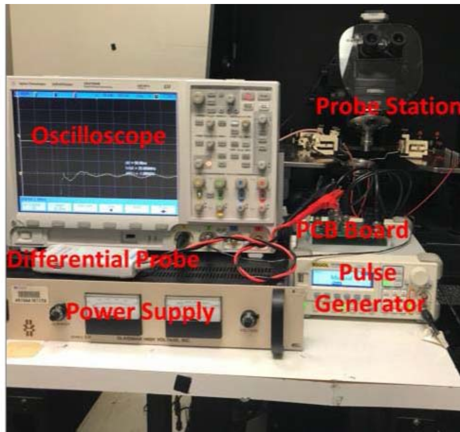

FIGURE 3. Measurement setup for the rectifier reverse recovery characteristics consists of an inductor, a MOSFET, an oscilloscope, a differential probe, a current probe, a pulse generator, and a probe station.

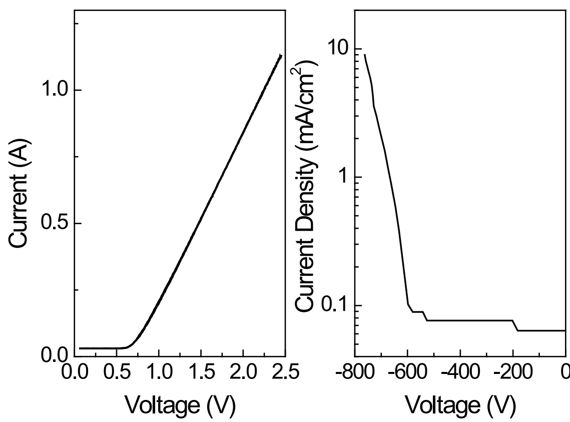

FIGURE 4. I-V characteristics from rectifier with area 7.85×10^{-3} cm^2.

was obtained as 4.36×10^{15} cm^{-3} from C-V characteristics. The on-state resistance, R_{ON}, was 22.2 mΩ.cm^2, leading to a power figure of merit (V_B^2 /R_{ON}) of 26 MW.cm^2. The diode on-off ratio was in the range 2.7 $\times$ 10^7-2.2 $\times$ 10^9 over our measurement range.

Figure 5 shows reverse recovery switching characteristics for a single device switching from 10V to -35V, with reverse recovery time, τ_{rr}, of 11 nsec. This was defined as the time taken for rectifiers recover to the current level of 25% of the reverse recovery current, I_{rr}. The reason for selecting 10 V is to get a forward current to be higher than 100 mA. Device size is 0.6 mm $\times$ 0.6 mm. This measurement shows intrinsic switching of the device without loading from a test circuit.

Figure 6 shows the switching performance and voltage waveform for the switching node of 1 A forward current/ 760 V rectifier. The device was switched from 1 A forward current to a reverse voltage of -300 V. The circuit was operated with a period of 100μsec, duty cycle 4%, MOSFET pulse was 10V and the power supply for the rectifier was 300V. The recovery time was 64 ns with I_{rr} of 0.82 A, and the dI/dt was 24.7 A/μs. The rectifier has a recovery time of

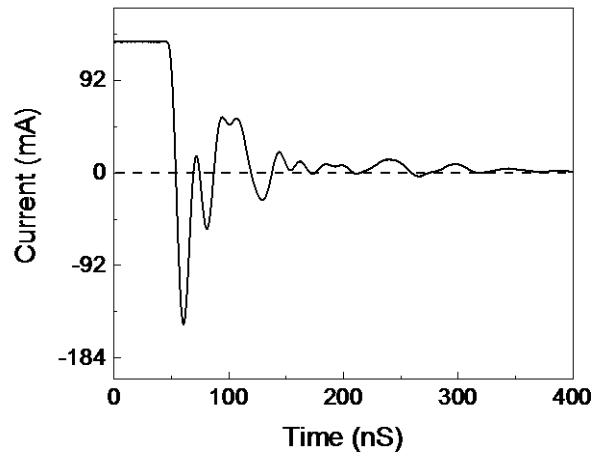

FIGURE 5. Switching for device only (no test circuit) from 10 V to -35 V, τ_{rr} = 11 nsec.

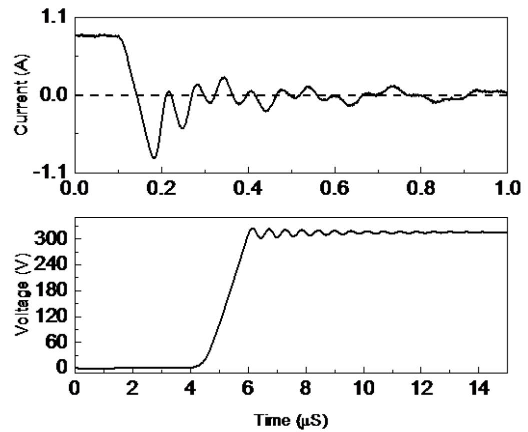

FIGURE 6. Rectifier switching from 1 A forward current to reverse off-state voltage of -300 V, showing τ_{rr} of 64 nsec voltage waveform on the switching node during the diode switching measurement.

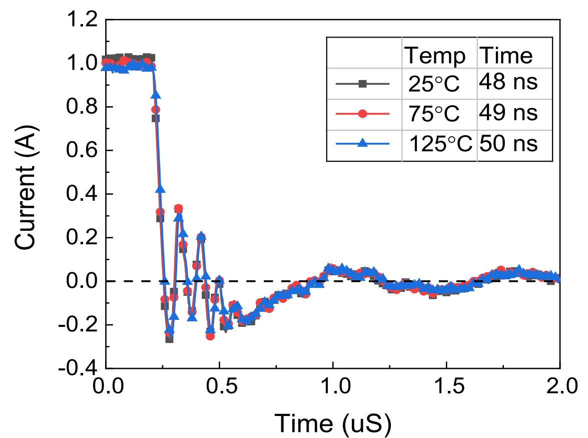

FIGURE 7. Temperature dependence of dynamic characteristics for rectifier switched from 1 A to reverse voltage of -200 V.

~11 ns- the additional recovery time comes from parasitics on the PCB board.

There is also interest in the switching performance at elevated temperatures since uncooled operation would be

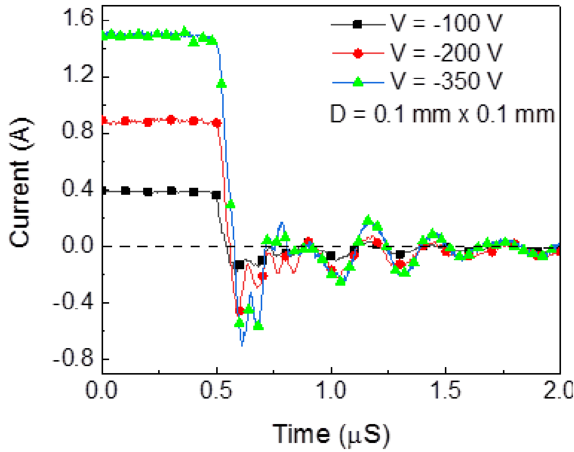

FIGURE 8. Effects of off-state switching voltage and on-state current on rectifier switching characteristics for different reverse voltage in a range of −100 V to −350 V.

an attribute of wide bandgap power switching systems. Figure 7 illustrates the effect of temperature on τ_{rr} for switching from 1A forward current to −200V reverse bias. Since the −300 V is the limit for these high current device switching, and to get repeatable experimental data, we decided to have devices switch up to −200 V for device protection. The τ_{rr} varied from 48 to 50 ns for 25 to 125°C. These are similar to the previous results reported for switching at much lower voltages (4V to 10V) [23]. There was no significant effect of either off state voltage or on-state current, a result of the short minority carrier lifetime of β-Ga_2O_3, as shown in Fig. 8. Lee *et al.* [26] reported the value of τ was 215 ps for Ga_2O_3 similar to the material used here. This was faster than the lifetime of ∼30 ns found in other studies [27], This indicates that the ultrafast radiative recombination reported by Lee *et al.* [26] may differ from that found at longer delay times. The lifetime reported applies to non-equilibrium holes in n-type β-Ga_2O_3.

TABLE 1. Summary of recovery characteristics of Ga_2O_3 FP RECTIFIER, Ga_2O_3 TRENCH MOSSBDs, Si-FRDs, and SiC-SBDs (after ref 25).

Device	I_{RRM} (A)	t_{rr} (nS)	Loss E_{rr} (μJ)	Reference
Si rectifier	1.85	25.6	0.12	[25]
SiC rectifier	0.43	7.6	1.66	[25]
Ga_2O_3 trench MOSSBD	0.42	7.6	0.09	[25]
Ga_2O_3 FP rectifier	0.70	64	1.52	This work

There are two types of turn-off power losses, namely turn-off losses in the diode and the switching losses induced by the diode turn-off during the MOSFET turn-on [28]. The latter value is shown in Table 1, along with a comparison of peak reverse recovery current (I_{RRM}), t_{rr} and recovery loss (E_{rr}) for previously reported Ga_2O_3 trench MOS Schottky diodes, Si-fast recovery diodes (FRDs, Rohm RF1005TF6S) and SiC Schottky barrier diodes from Cree (part number C3D0260A) [25] for turn-off from $I_F = 1$ A. The Err in our case is 1.52 uJ for diode turning-off only and around 18 uJ for total switching loss. For the Ga_2O_3 trench MOS-diode, the total switching loss is around 2 uJ. The main difference in these results is in the reverse voltage term on diode switching and reverse recovery charges Q_{rr} term. The diode in this work has $Q_{rr} = 30$ nC, while the trench MOS diode has $Q_{rr} = 3.2$ nC, which is the area under the curve of the first negative current peak. Our rectifiers are more than an order of magnitude larger area than the trench diodes and show comparable I_{RRM} and E_{rr} to state-of-the art SiC rectifiers.

These results demonstrate that Ga_2O_3 exhibits high speed switching characteristics. While the experimental values for blocking voltage are below the theoretical limits, continued developments in substrate defect reduction, epi-growth, device design, and fabrication processes will enhance its prospects for a role in power electronics. These results on large area rectifiers with high total current and an ability to operate in the >600V class range are another step in the advance of Ga_2O_3 for power electronics. Combined with the results from Takatsuka{25] on 1A, −100V trench MOS diode switching showing fast recovery from relatively large devices, these results confirm that Ga_2O_3 rectifiers are promising for power rectification applications. The immaturity, cost and limited variety are constrains for Ga_2O_3 being widely used in power switching applications. One possible solution to mitigate these issues might eventually be hybrid switches, a combination of Si MOSFETs and Ga_2O_3 rectifiers.

IV. SUMMARY AND CONCLUSION

β-Ga_2O_3 vertical Schottky rectifiers with an absolute forward current of >1 A and 760V breakdown voltage were demonstrated with large area (7.85×10^{-3} cm^2). These devices were switched from 1 A to −300 V with t_{rr} of 64 ns, an important milestone towards the applications of Ga_2O_3 rectifiers in high power switching technologies. The initial thrust on Ga_2O_3 electronics is targeted towards high power converters for both DC/DC and DC/AC applications. Ga_2O_3 Schottky diodes could supplement 600V Si or SiC rectifiers targeted at switch mode power converters.

REFERENCES

[1] A. Q. Huang, "Power semiconductor devices for smart grid and renewable energy systems," *Proc. IEEE*, vol. 105, no. 11, pp. 2019–2047, Nov. 2017, doi: 10.1109/JPROC.2017.2687701.

[2] T. P. Chow, I. Omura, M. Higashiwaki, H. Kawarada, and V. Pala, "Smart power devices and ICs using GaAs and wide and extreme bandgap semiconductors," *IEEE Trans. Electron Devices*, vol. 64, no. 3, pp. 856–873, Mar. 2017, doi: 10.1109/TED.2017.2653759.

[3] J. Millán, P. Godignon, X. Perpiñà, A. Pérez-Tomás, and J. Rebollo, "A survey of wide bandgap power semiconductor devices," *IEEE Trans. Power Electron.*, vol. 29, no. 5, pp. 2155–2163, May 2014, doi: 10.1109/TPEL.2013.2268900.

[4] M. Higashiwaki and G. H. Jessen, "The dawn of Ga_2O_3 microelectronics," *Appl. Phys. Lett.*, vol. 112, no. 6, 2018, Art. no. 060401, doi: 10.1063/1.5017845.

[5] S. J. Pearton *et al.*, "A review of Ga_2O_3 materials, processing, and devices," *Appl. Phys. Rev.*, vol. 5, no. 1, 2018, Art. no. 011301, doi: 10.1063/1.5006941.

[6] A. J. Green *et al.*, "3.8-MV/cm breakdown strength of MOVPE grown Sn-doped β-Ga_2O_3 MOSFETs," *IEEE Electron Device Lett.*, vol. 37, no. 7, pp. 902–905, Jul. 2016, doi: 10.1109/LED.2016.2568139.

[7] K. Zeng, A. Vaidya, and U. Singisetti, "1.85 kV breakdown voltage in lateral field-plated Ga_2O_3 MOSFETs," *IEEE Electron Device Lett.*, vol. 39, no. 9, pp. 1385–1388, Sep. 2018, doi: 10.1109/LED.2018.2859049.

[8] Y. Zhang *et al.*, "Demonstration of β-$(Al_xGa_{1-x})_2O_3/Ga_2O_3$ double heterostructure field effect transistors," *Appl. Phys. Lett.*, vol. 112, no. 23, 2018, Art. no. 233503, doi: 10.1063/1.5037095.

[9] M. H. Wong, K. Sasaki, A. Kuramata, S. Yamakoshi, and M. Higashiwaki, "Field-plated Ga_2O_3 MOSFETs with a breakdown voltage of over 750 V," *IEEE Electron Device Lett.*, vol. 37, no. 2, pp. 212–215, Feb. 2016, doi: 10.1109/LED.2015.2512279.

[10] J. Yang *et al.*, "High breakdown voltage (-201) β-Ga_2O_3 Schottky rectifiers," *IEEE Electron Device Lett.*, vol. 38, no. 7, pp. 906–909, Jul. 2017, doi: 10.1109/LED.2017.2703609.

[11] K. Konishi *et al.*, "1-kV vertical Ga_2O_3 field-plated Schottky barrier diodes," *Appl. Phys. Lett*, vol. 110, no. 10, 2017, Art. no. 103506, doi: 10.1063/1.4977857.

[12] K. Sasaki, M. Higashiwaki, A. Kuramata, T. Masui, and S. Yamakoshi, "Ga_2O_3 Schottky barrier diodes fabricated by using single-crystal β-Ga_2O_3 (010) substrates," *IEEE Electron Device Lett.*, vol. 34, no. 4, pp. 493–495, Apr. 2013, doi: 10.1109/LED.2013.2244057.

[13] O. Toshiyuki, K. Yuta, H. Kazuya, and K. Makoto, "High-mobility β-Ga_2O_3 (201) single crystals grown by edge-defined film-fed growth method and their Schottky barrier diodes with Ni contact," *Appl. Phys. Exp.*, vol. 8, no. 3, Feb. 2015, Art. no. 031101, doi: 10.7567/APEX.8.031101.

[14] J. Yang *et al.*, "High reverse breakdown voltage Schottky rectifiers without edge termination on Ga_2O_3," *Appl. Phys. Lett.*, vol. 110, no. 19, 2017, Art. no. 192101, doi: 10.1063/1.4983203.

[15] J. Yang, F. Ren, M. Tadjer, S. J. Pearton, and A. Kuramata, "2300V reverse breakdown voltage Ga_2O_3 Schottky rectifiers," *ECS J. Solid-State Sci. Technol.*, vol. 7, no. 5, pp. 92–96, 2017, doi: 10.1149/2.0241805jss.

[16] Q. He *et al.*, "Schottky barrier diode based on β-Ga_2O_3 (100) single crystal substrate and its temperature-dependent electrical characteristics," *Appl. Phys. Lett.*, vol. 110, no. 9, Feb. 2017, Art. no. 093503, doi: 10.1063/1.4977766.

[17] X. HuiWen *et al.*, "An overview of the ultrawide bandgap Ga_2O_3 semiconductor-based Schottky barrier diode for power electronics application," *Nanoscale Res. Lett.*, vol. 13, pp. 290–303, Sep. 2018. [Online]. Available: https://doi.org/10.1186/s11671-018-2712-1

[18] J. C. Yang, F. Ren, M. J. Tadjer, and A. Kuramata, "Vertical geometry, 2-A forward current Ga_2O_3 Schottky rectifiers on bulk Ga_2O_3 substrates," *IEEE Trans. Electron Devices*, vol. 65, no. 7, pp. 2790–2796, Jul. 2018, doi: 10.1109/TED.2018.2838439.

[19] J. Yang, F. Ren, M. Tadjer, S. J. Pearton, and A. Kuramata, "Ga_2O_3 Schottky rectifiers with 1 ampere forward current, 650 V reverse breakdown and 26.5 $MW.cm^{-2}$ figure-of-merit," *AIP Adv.*, vol. 8, no. 5, 2018, Art. no. 055026. [Online]. Available: https://doi.org/10.1063/1.5034444

[20] C. Joishi *et al.*, "Low-pressure CVD-grown β-Ga_2O_3 bevel-field-plated Schottky barrier diodes," *Appl. Phys. Exp.*, vol. 11, no. 3, pp. 1–5, 2018. [Online]. Available: https://doi.org/10.7567/APEX.11.031101

[21] I. Lee, A. Kumar, K. Zeng, U. Singisetti, and X. Yao, "Mixed-mode circuit simulation to characterize Ga_2O_3 MOSFETs in different device structures," in *Proc. IEEE 5th Workshop Wide Bandgap Power Devices Appl. (WiPDA)*, 2017, pp. 185–189, doi: 10.1109/WiPDA.2017.8170544.

[22] I. Lee, K. Zeng, U. Singisetti, and X. Yao, "Modeling and power loss evaluation of ultra wide band gap Ga_2O_3 devices for high power applications," in *Proc. IEEE Energy Convers. Congr. Expo. (ECCE)*, Cincinnati, OH, USA, Oct. 2017, pp. 4377–4382, doi: 10.1109/ECCE.2017.8096753.

[23] Q. He *et al.*, "Schottky barrier rectifier based on (100) β-Ga_2O_3 and its DC and AC characteristics," *IEEE Electron Device Lett.*, vol. 39, no. 4, pp. 556–559, Apr. 2018, doi: 10.1109/LED.2018.2810858.

[24] T. Funaki, T. Kimoto, and T. Hikihara, "Evaluation of high frequency switching capability of SiC Schottky barrier diode, based on junction capacitance model," *IEEE Trans. Power Electron.*, vol. 23, no. 5, pp. 2602–2611, Sep. 2008, doi: 10.1109/TPEL.2008.2002096.

[25] A. Takatsuka *et al.*, "Fast recovery performance of β-Ga_2O_3 trench MOS Schottky barrier diodes," in *Proc. 76th Device Res. Conf. (DRC)*, Santa Barbara, CA, USA, Jun. 2018, pp. 1–2, doi: 10.1109/DRC.2018.8442267.

[26] J. Lee *et al.*, "Effect of 1.5 MeV electron irradiation on β-Ga_2O_3 carrier lifetime and diffusion length," *Appl. Phys. Lett.* vol. 112, no. 8, 2018, Art. no. 082104, doi: 10.1063/1.5011971.

[27] L. Binet and D. Gourier, "Origin of the blue luminescence of β-Ga_2O_3," *J. Phys. Chem. Solids*, vol. 59, pp. 1241–1245, May 1998, doi: 10.1016/S0022-3697(98)00047-X.

[28] *Calculation of Turn-Off Power Losses Generated by a Ultrafast Diode*, STMicroelectronics, Geneva, Switzerland, 2017. [Online]. Available: https://www.st.com/resource/en/application_note/dm00380483.pdf

JIANCHENG YANG, photograph and biography not available at the time of publication.

FAN REN, photograph and biography not available at the time of publication.

YEN-TING CHEN, photograph and biography not available at the time of publication.

YU-TE LIAO, photograph and biography not available at the time of publication.

CHIN-WEI CHANG, photograph and biography not available at the time of publication.

JENSHAN LIN, photograph and biography not available at the time of publication.

MARKO J. TADJER, photograph and biography not available at the time of publication.

S. J. PEARTON, photograph and biography not available at the time of publication.

AKITO KURAMATA, photograph and biography not available at the time of publication.